

## EFFECTS OF AIR RESERVOIR VOLUME AND CONNECTING PIPES' LENGTH AND DIAMETER ON THE AIR SPRING BEHAVIOR IN RAIL-VEHICLES<sup>\*</sup>

H. SAYYAADI<sup>\*\*</sup> AND N. SHOKOUI

Dept. of Mechanical Engineering, Sharif University of Technology, Tehran, I. R. of Iran  
Email: sayyaadi@sharif.edu

**Abstract**— The secondary suspension of most new EMU and DMU rail vehicles is equipped with air springs, to offer a good ride comfort to passengers. Air springs are a very important isolating component, which guarantees good ride comfort during the trip. In most rail-vehicle models developed by researchers, the thermo-dynamical effects of air springs in the rail-vehicle dynamics are not considered and secondary suspension is modeled by simple springs and dampers. As the performance of suspension components, especially for air springs, have significant effects on rail-vehicle dynamics and the ride comfort of passengers, a complete nonlinear thermo-dynamical air spring model, which is a combination of two different models, is introduced. Results from field tests show remarkable agreement between the proposed model and experimental data. Effects of air reservoir volume and the connecting pipes' length and diameter on the system performances are investigated here.

**Keywords**— Rail vehicles, secondary suspension, air spring, parameters influences

### 1. INTRODUCTION

Most of the available works in the literature consider linear/nonlinear mechanical springs and dampers for the rail vehicle dynamics modeling. Sun and Dhanasekar [1] developed a 10 DOFs vehicle model with linear suspension components with four layer track models, and investigate the vertical dynamic interaction of subsystems in the longitudinal direction. To simulate the wheel/rail defects, Hou et al. [2] studied the effects of wheel/rail interactions by using the same vehicle model with an adaptive wheel/rail contact model, represented by a set of uniformly distributed linear springs. Tanabe et al. [3] and Zhang et al. [4] studied the interaction between railway structures and high speed trains by considering nonlinear characteristics for the suspension components. Tanabe et al. [3] developed a 31 DOFs vehicle model with nonlinear spring and damper describing functions. Durali and Bahabadi [5] developed a train model with 43 DOFs for studying train derailment in passing through bends. They considered the nonlinear behavior of suspension components and the effects of coupler forces in the vehicle dynamics. Li et al [6] studied the parameter identification problem for the rail vehicle suspensions with linear components. As they focused on the stability problem, only a half body plan view of the vehicle is modeled with 7 DOFs. Banerjee et al [7] developed a complete model for bolster bogies with 18 DOFs without considering the secondary suspension influences. In all of the mentioned works, the thermo-dynamical effects of air springs in the rail-vehicle dynamics are not considered and secondary suspension is modeled by mechanical springs and dampers.

Air springs, which are made of CBNFR rubber, have a long lifetime and they isolate the vehicle body from unpredictable noise and vibration. The air spring behaviors are so complicated that they cannot be

\*Received by the editors July 20, 2008; Accepted September 29, 2009.

\*\*Corresponding author

modeled by simple equations. The air spring response is independent of the excitation frequency [8] and it behaves as a stress relaxation function [9]. In addition, it has an asymmetric hysteresis loop, which is independent of the excitation frequency [10]. These behaviors bring difficulties for using a frictional or coulombic description to approximate the air spring characteristics. Stress relaxation function of CBNFR rubbers and the out of phase response of rail pads to different excitation frequencies are shown in Figs. 1 and 2.

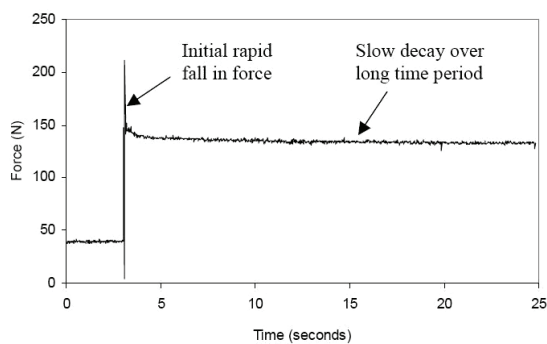


Fig. 1. Stress relaxation response [9]

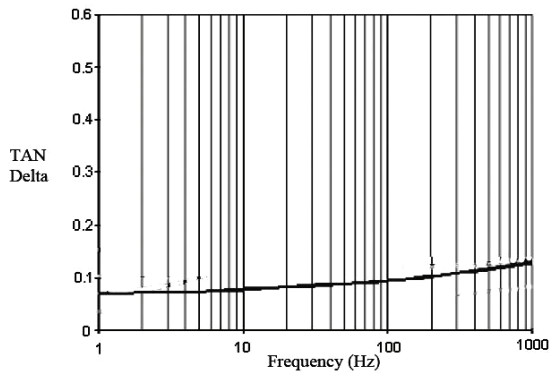


Fig. 2. Out of phase response of rail pad different excitation frequencies [8]

CBFNR response to cyclic excitation has asymmetric hysteresis loops, which are independent of the excitation frequency. This characteristic has been reported many times by different researchers [10, 11]. Figure 3 shows the typical asymmetric hysteresis loop of CBFNR rubbers.

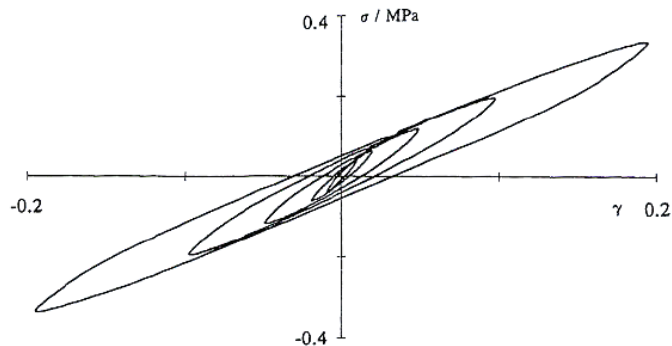


Fig. 3. CBFNR hysteresis loops [12]

## 2. AIR SPRING MODEL

For modeling CBFNR behavior, a model is introduced by Turner [12] and further developed by Coveney and Johnson [11]. In that model, named Triboelastic, a large number of microscopic, one dimensional, coulombic elements, linked by springs, are implemented in which the resulting friction force is proportional to the square root of current and previous turning point displacement differences.

Coveney and Johnson [13] modified the Triboelastic model and developed two new models named Triboelastic visco-solid (TVS) and Rate dependent Triboelastic (RT) model. The TVS is the same as the Berg model [10], while in the RT model, the Triboelastic element is replaced with a non-linear Maxwell element. TVS model has no asymmetric hysteresis loop, which causes rapid change in the force vector. Also, the model parameters cannot easily be adjusted.

Bergstrom and Boyce [14] developed a different model similar to the Triboelastic RT model with two differences; equilibrium response is described by a hyper-elastic model and time dependent response is a

function of both velocity and displacement raised to a power. This model still has some difficulties to implement in the dynamic analysis.

Miehe and Keck [15] introduced a model similar to the Berg and TVS model. This model has 20 parameters, which made it very difficult to define the values of all of the parameters.

Lion [16] proposed a phenomenological model with non-linear elasticity, non-linear plastic hysteresis, non-linear visco-elasticity and stress softening which has modular components, the same as the Miehe and Keck model, but is different in functions. The equations given for this model are very difficult to implement in the dynamic analysis.

In the latest 3D model, developed by Berg [17], the effects of elasticity, friction and viscosity of air spring in the vertical, lateral and longitudinal directions are introduced. In that model, the stress relaxation response is not represented. A complete explanation about this model, shown in Fig. 4, can be found in [17]. Friction force in this model is defined by the following function, which is zero at the turning points.

$$F_{Friction} \propto \frac{(x - x_0)}{\beta + (x - x_0)} sign(\dot{x}) \quad (1)$$

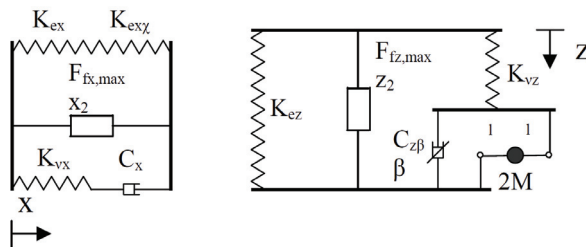


Fig. 4. Berg model [17]

In the above equation,  $\beta$  is constant,  $x$  is current displacement and  $x_0$  is the displacement at the previous turning point. It can be seen that in this model, displacement at the turning points should be detected and assigned to the  $x_0$  variable, which is not a standard procedure in the dynamic analysis and causes failure in solving the algorithm.

For simulation of CBFNR rubber behavior, a model was developed by Haupt & Sedlan [9] which has elastic and viscoelastic elements. The viscoelastic element naturally produces an asymmetric stress-strain response and is weakly time-dependent. These features are not presented in the other models, and so made it very powerful for simulating the CBFNR behaviors. Simplified one-dimensional Haupt & Sedlan model with constant coefficients is shown in Fig. 5.

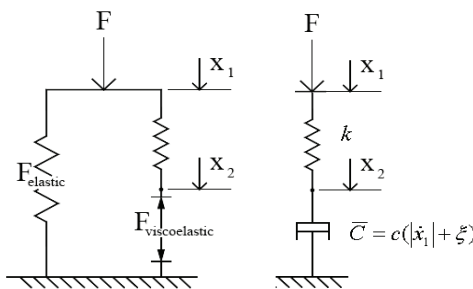


Fig. 5. One-dimensional Haupt & Sedlan model

The simplified viscoelastic force in this model is described by the following function:

$$F_{visco-elastic} = \frac{c \dot{x}_2}{|\dot{x}_1| + \zeta} \quad (2)$$

Where  $c$  and  $\zeta$  are constant. Eq. (2) is simply a standard linear Maxwell element where the viscous force is divided into the magnitude of strain rate and a constant.

In this research work, the Berg model, which is validated by some experimental excitation data up to 16 Hz frequencies [17], is used to simulate air spring behaviors. However, because of difficulties comprised from assigning the previous turning point displacement to the variable, the frictional part of this model is replaced by the simplified viscoelastic model defined by Haupt & Sedlan. Schematic diagrams of the modified models in the vertical and lateral directions are shown in Fig. 6.

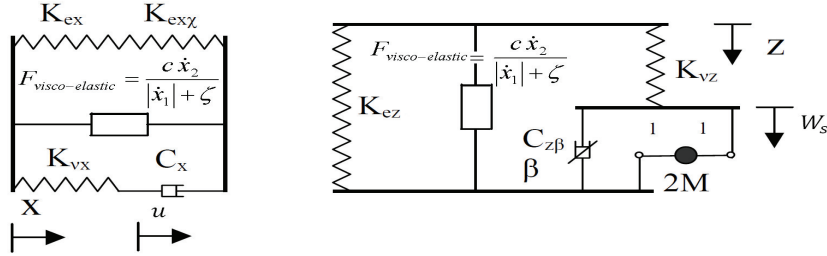


Fig. 6. Proposed modified model for air spring

According to Berg, and by taking into consideration the Haupt & Sedlan model, differential equations of air spring behavior in vertical, lateral and longitudinal directions are determined as follows:

Vertical direction:

$$M \ddot{w}_s = K_{vz}(z - w_s) - C_{z\beta} |\dot{w}_s|^\beta \text{sign}(\dot{w}_s), \quad \beta = 1.8 \quad (3)$$

$$F_z = (p_0 - p_a)A_e + K_{ez}z + K_{vz}(z - w_s) + \frac{c \dot{x}_2}{|\dot{z}| + \zeta}$$

Lateral and longitudinal directions:

$$F_w = K_{ew}w + K_{ew\chi}\theta + F_{visco-elastic,w} + K_{vw}(w - u) \quad (4)$$

$$C_w \dot{u} = K_{vw}(w - u)$$

And

$$F_{visco-elastic,w} = \frac{c \dot{x}_2}{|\dot{w}_1| + \zeta}, \quad w = x, y \quad (5)$$

Numerical values of the above parameters are estimated by the following equations [18]:

$$M = l_s A_s \rho \left( \frac{A_e}{A_s} \frac{V_{r0}}{V_{b0} + V_{r0}} \right)^2$$

$$K_{ez} = \left( \frac{1}{\frac{p_0 A_e^2 n}{V_{b0} + V_{r0}} + p_g \frac{dA_e}{dz}} + \frac{1}{K_{auxiliary}} \right)^{-1} \quad (6)$$

$$K_{vz} = \left( \frac{1}{\frac{p_0 A_e^2 n}{V_{b0}} + p_g \frac{dA_e}{dz}} + \frac{1}{K_{auxiliary}} \right)^{-1} - K_{ez}$$

$$C_{z,\beta} = \frac{1}{2} \rho \cdot k_t \cdot A_s \left( \frac{A_e}{A_s} \frac{V_{r0}}{V_{b0} + V_{r0}} \right)^{1+\beta}, \quad \beta = 2$$

The exact  $C_{z,1.8}$  value is calculated based on the Presthus method and the stiffness  $K_{exz}$  can be approximated by  $K_{exz} = 0.7(K_{ex}h + load)$  [18]. The parameters of IRICO DMU air springs in the above equations are described in Table 1.

Table 1. Air spring parameters value

Parameters	Description	Values
$l_s$	Connecting pipe length	3.2 m
$A_s$	Connecting pipe cross section	0.001359 m <sup>2</sup>
$A_e$	Effective area of the air spring	0.291 m <sup>2</sup>
$P_0$	Initial absolute air spring pressure	3.806 bar
$P_g$	Gauge pressure	-
$\rho$	Density of the air at $P_0$ pressure	4.523 kg/m <sup>3</sup>
$V_{r0}$	Reservoir volume	0.040 m <sup>2</sup>
$V_{b0}$	Air spring volume	0.064 m <sup>2</sup>
$k_t$	Total lost coefficient of connection pipes	3.4727
$K_{auxiliary}$	Auxiliary spring stiffness in air spring	8234 kN/m
$M$	Air mass	198.385 kg

### 3. MODEL SIMULATION

To evaluate the performance of the equations, the model is developed in Matlab/Simulink software. Figure 7 shows the proposed model for one IRICO DMU air spring in a Simulink environment.

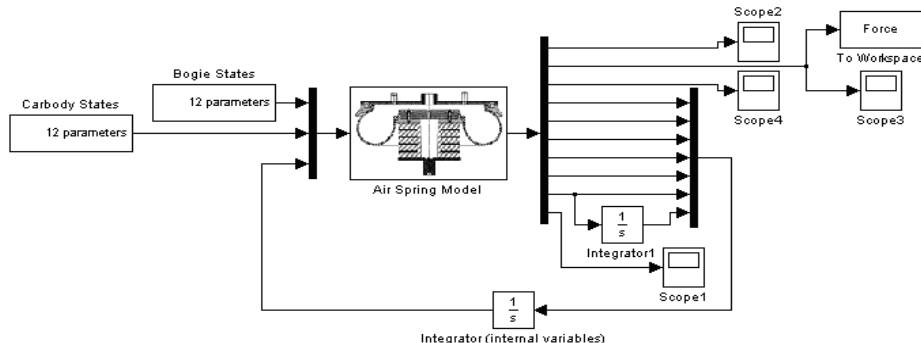


Fig. 7. Developed model for air spring simulation

For evaluating the performance of the developed model, bogie states are fixed to constant and response of air spring to sinusoidal movement of carbody in vertical and lateral directions as shown in Fig. 8 are studied. Responses of air spring in vertical and lateral directions are shown in Fig. 9.

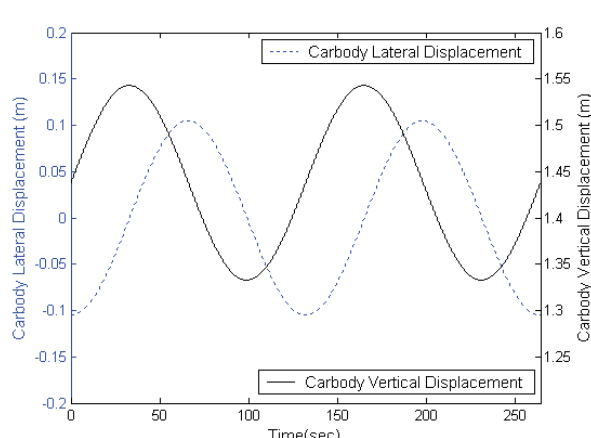


Fig. 8. Reference vertical and lateral carbody displacement

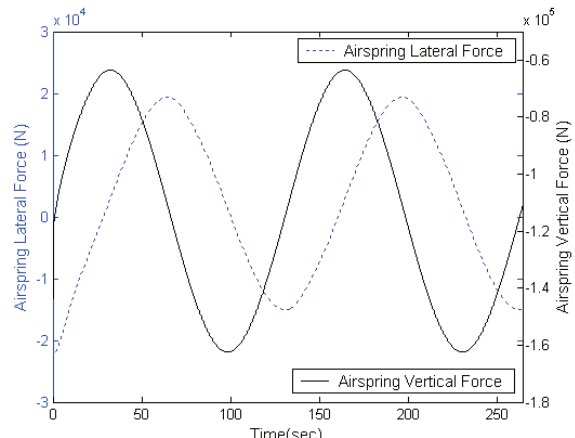


Fig. 9. Vertical and lateral reaction force of air spring

#### 4. EXPERIMENTAL RESULTS

To determine the exact value of the air spring parameters, a real test of an IRICO DMU air spring is carried out at ContiTech Company, Germany. The test was carried out according to the EN13597 standard at 109.8 KN vertical load with an amplitude of  $\pm 10 \text{ mm}$  and between 0.5 and 10 Hz frequencies. The length and diameter of the hoses between the air spring and the auxiliary volume and the other air suspension specifications are chosen so that these values agree with the rail vehicle design. Figure 10 depicts the air spring test.

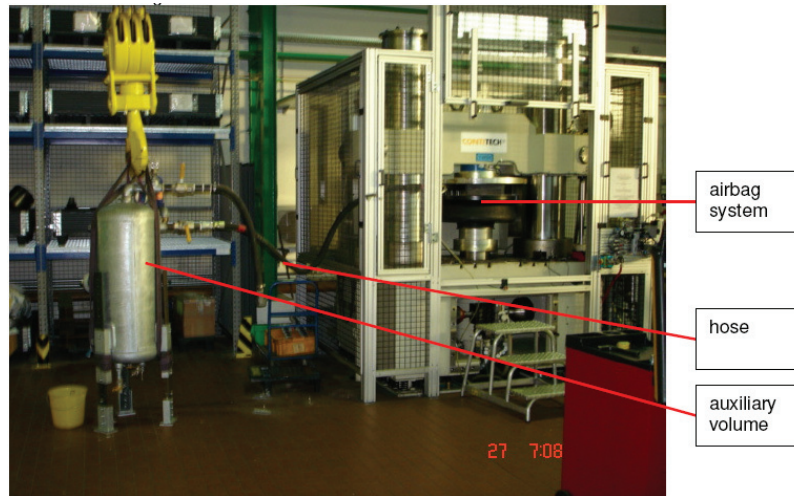


Fig. 10. Test rig of air spring at ContiTech Company, Germany

Based on the method introduced by Docquier [19], loss angle and vertical dynamic stiffness of the air spring, as shown in Figs. 11 and 12, are investigated.

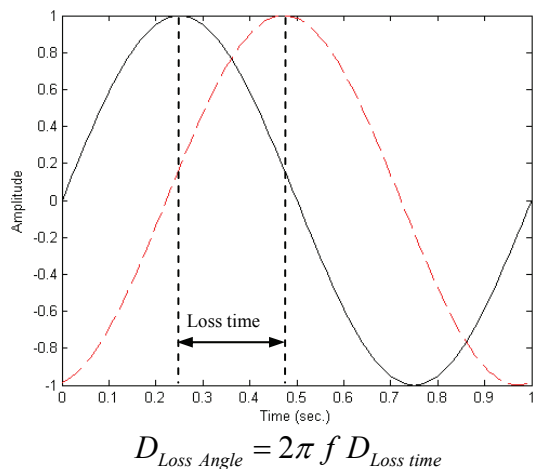


Fig. 11. Loss angle

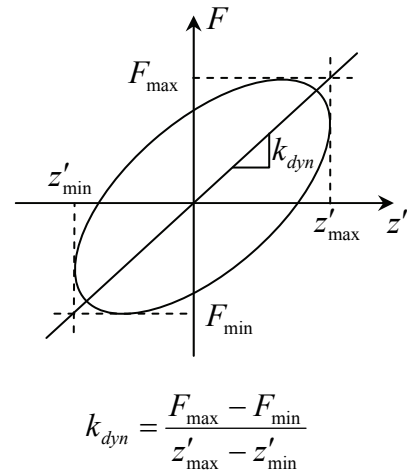


Fig. 12. Dynamic vertical stiffness [19]

According to the real test data and simulation results, the loss angle and vertical dynamic stiffness of the air spring are calculated and shown in Figs. 13 and 14. As can be seen, good agreement between the real test and the simulation results is achieved.

To validate the lateral behavior, the hysteresis loop of the air spring is evaluated. Results are shown in Fig. 15. Good agreement between the real test and the simulation results shows that the proposed equations can simulate the real behavior of the air spring very well.

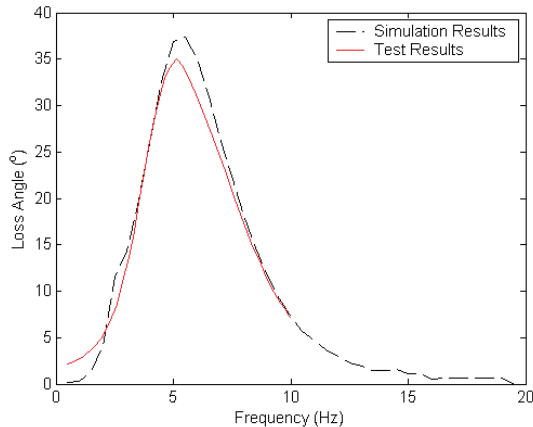


Fig. 13. Loss angle of the air spring

$$\begin{aligned} M &= 198.385 \text{ kg}, K_{ez} = 461.629 \text{ N/mm} \\ K_{vz} &= 351.185 \text{ N/mm}, C_{z,1.8} = 11.508 \text{ kN(s/m)}^{1.8} \\ k_{\text{haupt}} &= 96 \text{ kN/m}, C_{\text{haupt}} = 1.52 \text{ kNs/m}, \zeta = 0.00063 \end{aligned}$$

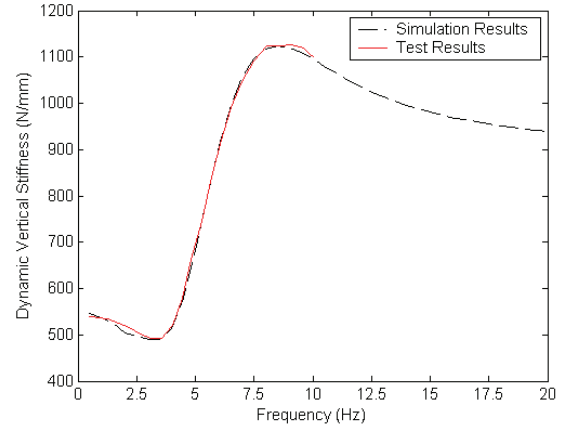


Fig. 14. Dynamic vertical stiffness of the air spring

$$\begin{aligned} M &= 198.385 \text{ kg}, K_{ez} = 461.629 \text{ N/mm} \\ K_{vz} &= 351.185 \text{ N/mm}, C_{z,1.8} = 11.508 \text{ kN(s/m)}^{1.8} \\ k_{\text{haupt}} &= 96 \text{ kN/m}, C_{\text{haupt}} = 1.52 \text{ kNs/m}, \zeta = 0.00063 \end{aligned}$$

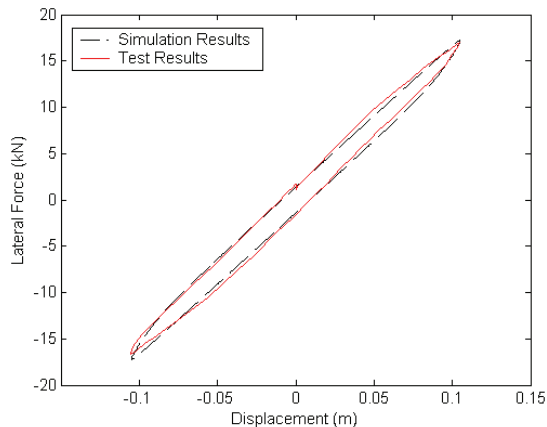


Fig. 15. Hysteresis loop of the air spring in lateral direction

$$\begin{aligned} K_{ey} &= 154 \text{ kN/m}, K_{vy} = 82.26 \text{ kN/m}, C_y = 1.109 \text{ kNs/m} \\ k_{\text{haupt}} &= 96 \text{ kN/m}, C_{\text{haupt}} = 1.52 \text{ kNs/m}, \zeta = 0.00063 \end{aligned}$$

## 5. AIR RESERVOIR VOLUME AND CONNECTING PIPES' INFLUENCES

In this section, the influence of rail–vehicle secondary suspension parameters on the performance of the air spring, including air reservoir volume and the connecting pipes' length and diameter, will be discussed.

### a) Air reservoir volume

Performance of air springs is highly affected by air reservoir volume. For studying the influences of air reservoir volume on the system performances, the dynamic stiffness and loss angle of the air spring reaction force for various air reservoir volumes are studied within 0~20 Hz excitation frequencies as shown in Figs. 16 and 17. As it can be seen, by adjusting the air reservoir volume to zero, the air spring behaves as a simple stiffness component and the loss angle of the reaction force is zero for all excitation frequencies. This indicates that no damping characteristic exists in the system when the air reservoir volume is zero.

By increasing the air reservoir volume, the dynamic stiffness graph is divided into low, transient and high frequency sections and the damping characteristic is appended to the system in the shape of a loss

angle within a specific frequency range. At the same time, the maximum loss angle occurs at lower frequencies with a higher amplitude, as increasing the air reservoir volume from 5 to 80 liters increases maximum loss angle from  $15.7^\circ$  at 14.5 Hz to  $48.1^\circ$  at 4 Hz frequency.

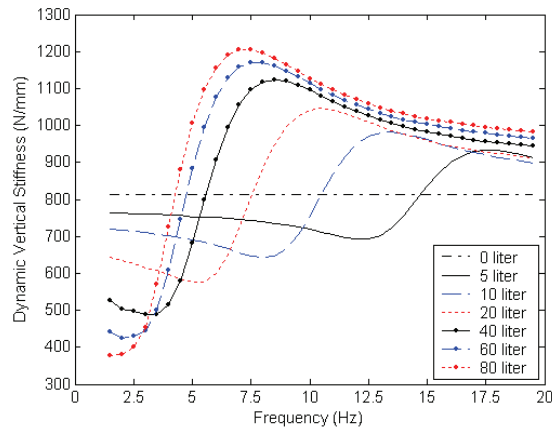


Fig. 16. Dynamic vertical stiffness of air spring for various air reservoir volumes

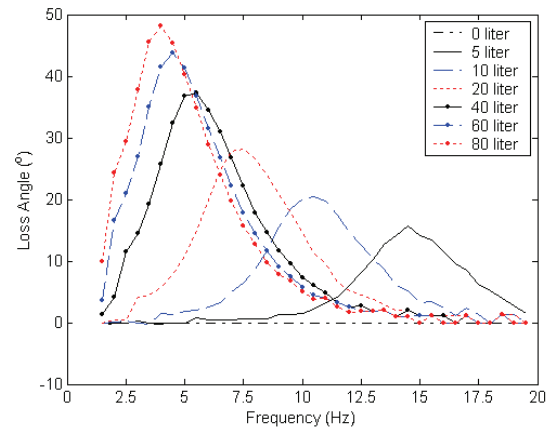


Fig. 17. Loss angle of air spring for various air reservoir volumes

Furthermore, when the air reservoir volume is increased, the dynamic stiffness of the system is decreased at low frequencies and increased at high frequencies. In the same way and as can be seen in Fig. 17, the maximum loss angle also occurred at lower frequencies. So, by identifying the resonance frequency of the rail-vehicle, the transient section of the air spring response can be adjusted so that vehicle responses are restricted.

#### b) Connecting pipe diameter

As seen in Fig. 18, by increasing the connecting pipe diameter, the transient section of the air spring dynamic stiffness is shifted to higher frequencies. The same concept is valid for the loss angle, as shown in Fig. 19. By increasing the connecting pipe diameter, the maximum loss angle is shifted to higher frequencies with higher amplitude.

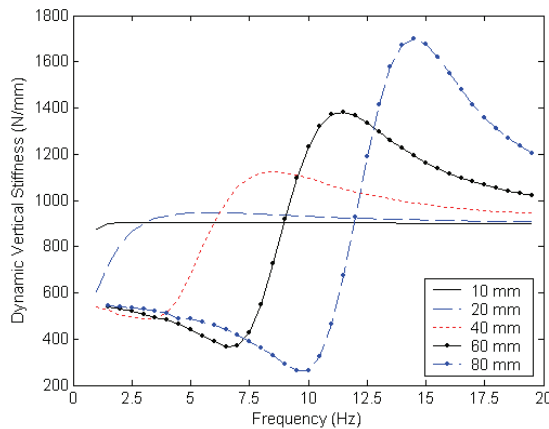


Fig. 18. Dynamic vertical stiffness of air spring for various pipe diameters

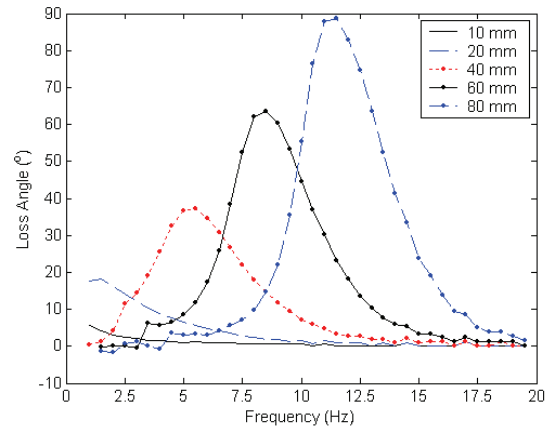


Fig. 19. Loss angle of air spring for various pipe diameters

Whereas increasing the air reservoir volume shifts the graphs to the lower frequencies, increasing the connecting pipe diameter shifts the graphs to the higher frequencies. Comparing the reservoir volume and the connecting pipe diameter influences shows that both factors add a damping characteristic to the system.

### c) Connecting pipes' length

Dynamic stiffness and loss angle of air spring for different connecting pipe lengths are shown in Figs. 20 and 21. By increasing the connecting pipes' length, the dynamic stiffness and loss angle graphs are widened. As can be seen, for all connecting pipe lengths, the low frequency section remained unchanged. Furthermore, the transient section is widened and the high frequency section is shifted to higher frequencies.

So by adjusting connecting pipes' length, damping characteristic of air spring can cover wider range of excitation frequencies.

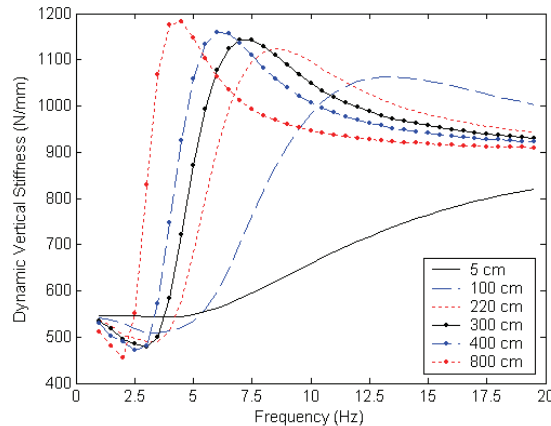


Fig. 20. Dynamic vertical stiffness of air spring for various pipe lengths

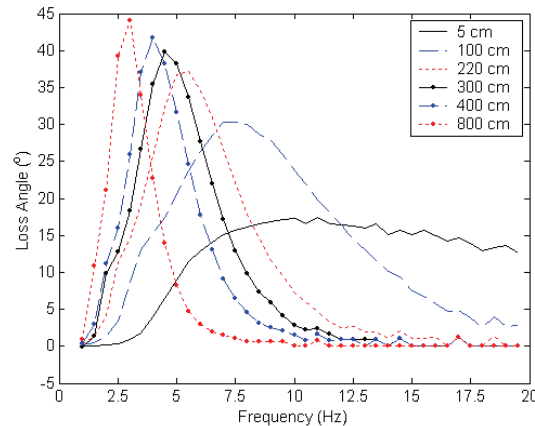


Fig. 21. Loss angle of air spring for various pipe lengths

## 6. CONCLUSION

This research work proposes a new nonlinear air spring model for studding air suspension components influences on the system behavior. This new model is validated by using real test data from field experiments and can be easily used in the dynamic modeling of air springs. Comparison of the results shows good agreement between the proposed model and the test results, indicating this new model can be used for simulation of secondary suspension behaviors very well, and so it is a good model for further applications such as improvement in ride quality and comfort index. Effects of air reservoir volume and the connecting pipes' length and diameter on the system performances are investigated. By estimating proper values for these three air suspension parameters and based on the design requirements in rail-vehicles, good satisfaction of the suspension system will be achieved.

**Acknowledgments:** The authors are grateful for the considerable support from Irankhodro Rail Transport Industries Co. and would also like to express their sincere thanks to Mr. N. Soofi for his support.

## REFERENCES

1. Sun, Y. Q. & Dhanasekar, M. (2002). A dynamic model for the vertical interaction of the rail track and wagon system. *International Journal of Solids and Structures*, Vol. 39, pp. 1337–1359.
2. Hou, K., Kalousek, J. & Dong, R. (2003). A dynamic model for an asymmetrical vehicle/track system. *Journal of Sound and Vibration*, Vol. 267, pp. 591–604.
3. Tanabe, M., et al. (2003). Computational model of a Shinkansen train running on the railway structure and the industrial applications. *Journal of Materials Processing Technology*, Vol. 140, pp. 705–710.

4. Zhang, N., Xia, H., et al (2008). Vehicle–bridge interaction analysis under high-speed trains. *Journal of Sound and Vibration*, Vol. 309, pp. 407–425.
5. Durali, M. & Bahabadi, M. M. J. (2004). Investigation of train dynamics in passing through curves using a full model. *Rail Conference, Proceedings of the ASME/IEEE Joint*, pp. 83–88.
6. Li, P., Goodall R., et al. (2007). Estimation of railway vehicle suspension parameters for condition monitoring. *Control Engineering Practice*, Vol. 15, pp. 43–55.
7. Banerjee, N., et al (2008). Bond graph modeling of a railway truck on curved track. *Simulation Modeling Practice and Theory*, Available online.
8. Boast, D., Fellows, S. & Hale M. (2002). Effects of temperature, frequency and amplitude on the dynamic properties of elastomers. *AVON Automotive Conference*, 03.
9. Haupt, P. & Sedlan, K. (2001). Viscoplasticity of elastomeric materials: experimental facts and constitutive modeling. *Archive of Applied Mechanics*, Vol. 71, pp. 89-109.
10. Berg, M. (1998). A non-linear rubber spring model for rail vehicle dynamics analysis. *Journal of Vehicle system dynamics*, Vol. 30, pp. 197-212.
11. Coveney, V. A., Johnson, D. E. & Turner, D. M. (1995). A triboelastic model for the cyclic mechanical behaviour of filled vulcanizates. *Journal of Rubber Chemistry and technology*, Vol. 68, pp. 660-670.
12. Turner, D. M. (1988). A triboelastic model for the mechanical behaviour of rubber. *Journal of Plastics and Rubber Processing and Applications*, Vol. 9, pp. 197-201.
13. Coveney, V. A. & Johnson, D. E. (2000). Rate-dependent modelling of a highly filled vucanizate. *Journal of Rubber Chemistry and technology*, Vol. 73, No. 4, pp. 565-577.
14. Bergstrom, J. S. & Boyce, M. C. (2000). Large strain time-dependent behavior of filled elastomers. *Journal of Mechanics of Materials*, Vol. 32, pp. 627-644.
15. Miehe, C. & Keck, J. (2000). Superimposed finite elastic-viscoelastic-plastoelastic stress response with damage in filled rubbery polymers Experiments, modelling and algorithmic implementation. *Journal of Mechanics and Physics of Solids*, Vol. 48, pp. 323-365.
16. Lion, A. (1996). A constitutive model for carbon black filled rubber: Experimental investigation and mathematical representation. *Journal of Continuum Mechanics and Thermodynamics*, Vol. 8, pp. 153-169.
17. Berg, M. (1999). A three-dimensional airspring model with friction and orifice damping. *Journal of Vehicle System Dynamics*, Vol. 33, pp. 528–539.
18. Presthus, M. (2002). Derivation of air spring model parameters for train simulation. Master dissertation, Department of Applied Physics and Mechanical Engineering, Division of Fluid Mechanics, LULEA University.
19. Docquier, N., Fisette, P. & Jeanmart, H. (2007). Multiphysic modelling of railway vehicles equipped with pneumatic suspensions. *Journal of Vehicle System Dynamics*, Vol. 45, No. 6, pp. 505–524.